Society For Biomaterials

An *in vitro* and *in vivo* characterization of fine WE43B magnesium wire with varied thermomechanical processing conditions

Adam J. Griebel,[1] Jeremy E. Schaffer,[1] Tracy M. Hopkins,[2] Alaa Alghalayini,[2] Tinomudaishe Mkorombindo,[2] Kolade O. Ojo,[3] Zhigang Xu,[4] Kevin J. Little,[5] Sarah K. Pixley[2]

[1]Research & Development, Fort Wayne Metals Research Products Corp, Fort Wayne, Indiana
[2]Department of Pharmacology and Systems Physiology, University of Cincinnati College of Medicine, Cincinnati, Ohio
[3]Department of Chemistry, University of Cincinnati College of Arts & Sciences, Cincinnati, Ohio
[4]Department of Mechanical Engineering, North Carolina A&T State University, Greensboro, North Carolina
[5]Department of Orthopaedic Surgery, Division of Pediatric Orthopaedics, Cincinnati Children's Hospital Medical Center, Cincinnati, Ohio

Received 25 February 2017; revised 5 September 2017; accepted 11 September 2017
Published online 00 Month 2017 in Wiley Online Library (wileyonlinelibrary.com). DOI: 10.1002/jbm.b.34008

Abstract: Absorbable implants made of magnesium alloys may revolutionize surgical intervention, and fine magnesium wire will be critical to many applications. Functionally, the wires must have sufficient mechanical properties to withstand implantation and in-service loading, have excellent tissue tolerance, and exhibit an appropriate degradation rate for the application. Alloy chemistry and thermomechanical processing conditions will significantly impact the material's functional performance, but the exact translation of these parameters to implant performance is unclear. With this in mind, fine (127 μm) WE43B magnesium alloy wires in five thermomechanical process (TMP) conditions (90% cold work [CW], and 250, 375, 400, and 450°C heat treatments) were investigated for their effect on mechanical and corrosion behavior. The TMP conditions gave clear metallurgical differences: transverse grain dimensions ranged from 200 nm (CW) to 3 μm (450°C), UTS varied from 324 MPa (450°C) to 608 MPa (250°C), and surgical knotting showed some were suitable (CW, 400°C, 450°C) while others were not (250°C, 350°C). *In vitro* and *in vivo* corrosion testing yielded interesting and in some cases conflicting results. After 1 month immersion in cell culture medium, wire corrosion was extensive, and TMP conditions altered the macrocorrosion morphology but not the rate or total release of magnesium ions. After 1 month subdermal implantation in mice, all wires were well tolerated and showed very little corrosion (per μCT and histology), but differences in localized corrosion were detected between conditions. This study indicates that WE43B wires treated at 450°C may be most suitable for surgical knotting procedures. © 2017 Wiley Periodicals, Inc. J Biomed Mater Res Part B: Appl Biomater 00B: 000–000, 2017.

Key Words: magnesium, biodegradable metal, thermomechanical processing, wire, WE43B alloy

How to cite this article: Griebel, AJ, Schaffer, JE, Hopkins, TM, Alghalayini, A, Mkorombindo, T, Ojo, KO, Xu, Z, Little, KJ, Pixley, SK 2017. An *in vitro* and *in vivo* characterization of fine WE43B magnesium wire with varied thermomechanical processing conditions. J Biomed Mater Res Part B 2015:00B:000–000.

INTRODUCTION

Magnesium (Mg) has several properties that make it attractive for use as a biomedical implant material. Key among these are that its hardness and mechanical strength can closely mimic hard tissue properties and that implantation is followed by apparently benign, and even tissue-promoting, biodegradation under the appropriate conditions.[1–3] A safe biodegradable material is desirable in a large number of injury paradigms, where the implant can provide physical support and then disappear after the regenerating tissues achieve self-support. In terms of safety and clinical use, while Mg is not currently FDA approved as an implant material in the United States, a Mg screw for fixation of the big toe has been given CE mark in Europe and is being sold and used clinically there.[2–4] Additionally, Mg-based cardiovascular stents are performing well in clinical trials in Europe.[2,5]

While a major focus for Mg implants is its use in bone, where the desired parameter is strength, other applications are to provide physical support in soft tissues, like repairs of blood vessels, nerves, or other tissues. Multiple applications could benefit from the use of Mg wires that would hold injured tissues together, temporarily and initially, providing more strength than some conventional materials, and then safely degrade, avoiding interference with further

Additional Supporting Information may be found in the online version of this article.
Portions of this work have appeared previously in abstract and poster form.
Correspondence to: S. K. Pixley, e-mail: Pixleysk@ucmail.uc.edu
Contract grant sponsor: NSF Engineering Research Center (ERC) for Revolutionizing Metallic Biomaterials; contract grant number: NSF EEC 0812348

healing. An example is our recent exploration to use the physical strength of Mg wire to support nerve regeneration across a nerve injury gap.[6] In this application and in any other potential soft tissue situations, it is desirable to engineer Mg to mimic the flexural stiffness of the soft tissues thereby preventing potentially harmful mechanical mismatch.

When compared to metals commonly used in the medical field, such as stainless steel (SS) or titanium, Mg and its alloys have relatively low ductility at room temperature. Generally, this means metalworking of magnesium material is performed at elevated temperatures (>250°C) to avoid cracking. However, recent work to develop room temperature, or cold, wire drawing techniques for magnesium alloys has resulted in wires with strengths, diameters, and surface finishes suitable for the medical device industry.[7–9] Furthermore, the wire thermomechanical process (TMP) conditions and tight tolerance geometries can be tuned to influence the material flexibility and drive desirable mechanics for various tissue situations.[7–9]

In addition to the difficulties of manufacturing Mg wire, other issues are that Mg is a relatively soft material and may not maintain its physical strength for a particular application, and that Mg may not resist resorption long enough to support healing if it is weakened by respective implantation and service loads. Furthermore, Mg absorption in the body is influenced by a complicated mix of factors that include temperature, type of fluid, and amount of fluid in tissues. When Mg degrades in aqueous solutions, the metal reacts with water to produce hydroxyl ions and hydrogen gas. Release of hydrogen and associated tissue bubble formation can be mitigated by engineering the material to slow the resorption rate.[10] Thus, current challenges in developing Mg as an implant material are to control both the strength and corrosion rate.

The primary mode to increase strength and reduce corrosion rate is through alloying. For biomedical uses, the alloying elements should be nontoxic in the quantities expected to be released from the implant. One alloy, WE43B, originally developed for aerospace applications, has shown good potential as an absorbable metal with good strength, ductility, and corrosion properties.[4,5,11–13] The alloy, containing nominally 4 wt % Y, 3 wt % rare earths, and 0.5 wt % Zr, has generally shown an acceptable *in vitro* and *in vivo* response.[4,5,11–13]

Once a particular alloy chemistry has been established, the thermal and mechanical processes used to manufacture it into the required form will have a large impact on performance. More research is needed to understand the effects of processing. It is generally understood in the literature that the microstructure of magnesium alloys will influence their corrosion behavior.[14] However, as noted earlier, cold-drawn magnesium alloy wire has only been recently developed for medical applications. As such, the literature lacks a detailed investigation on the corrosion behavior of these fine wires with various TMPs. Consequently, a key aim here was to provide a first look at the corrosion behavior of fine (127 μm diameter) WE43B wires prepared using five TMP conditions. Specifically, wires were subjected to tensile testing, microstructural evaluation, surgical handling and knotting, and *in vitro* and *in vivo* corrosion tests, with an aim to inform suitability for medical uses.

METHODS

Production of WE43B wire

WE43B wires of 127 μm diameter were produced using good manufacturing practices and conventional cold-drawing techniques, employing oil-based lubricants and natural diamond drawing dies to deliver a bright surface finish. Wires of 400 μm diameter were annealed at 450°C and directly cold drawn to 127 μm to achieve 90% cold work (CW), where CW is given as a percent reduction of area, as shown in Eq. (1). Cold working metals results in strength increases, primarily through stored internal energy, for example, by the accumulation of dislocations in the microstructure.

$$\text{cold work} = 1 - \left(\frac{d_f}{d_i}\right)^2 \tag{1}$$

Heat treatment after cold working can induce several phenomena, such as precipitation of secondary phases, recovery of dislocations, recrystallization of new grains, and/or grain growth, depending on the heat treatment parameters.[15] After cold drawing, the material was allocated into five TMP condition groups. The first condition received no further processing and the wire was left in the cold-worked state. The second condition (250°C) was treated at 250°C, to produce an aging response through precipitation-hardening.[15] The third condition (375°C) was thermally treated at 375°C, providing an expected balance of precipitation-hardening and recovery of cold-work-induced dislocations. The fourth condition (400°C) was thermally treated at 400°C, with the aim of achieving recovery and recrystallization with limited grain growth. The fifth and final condition (450°C) was annealed at 450°C and was expected to allow some grain growth to produce a larger size than the 400°C.

Microstructural assessment

To allow observation of the microstructure, samples of the wires were polished on Al_2O_3 films with a Multiprep Polishing System (Allied High Tech Products, Inc. USA). After polishing, the Mg alloy wires were etched using 5% nital solution (5% nitric acid in methanol); the SS wire was etched with Kalling' No. 2 solution (12 g cupric chloride, 20 mL hydrochloric acid, and 225 mL alcohol). The microstructural images were acquired with a cold cathode field emission scanning electron microscope (FESEM, SU8000, Hitachi) with a combination of secondary and backscattering electrons.

Tensile testing

Mechanical properties of wires in the various TMP conditions were assessed via tensile testing using an Instron 5966 frame (Instron, Norwood, MA) equipped with a 100 *N* load cell. Specific parameters included: gauge length = 127 mm, strain rate = 0.0033 s^{-1}, $N = 3$ per condition. Measured properties

included yield strength, ultimate tensile strength, elongation at fracture, and elastic modulus.

Surgical handling assessment

An experienced surgeon compared the surgical handling capabilities of the wires against his experience with similar sized standard sutures (nonabsorbable: between 5–0 = 0.1 mm diameter and 4–0 = 0.15 mm diameter), by tying wires around a fixed support, by hand or using a needle driver. Standard sutures easily allow tying approximately 3–4 knots under these conditions.

Wire corrosion *in vitro*

Mg wires were cut (SS razor blades) into 1 cm segments, sterilized with 100% ethanol, air dried under UV light in a sterile environment and placed, one per well, in a 12 well tissue culture plate. Wells were filled with 1 mL of DMEM culture medium with 10% fetal calf serum (Hyclone; Thermo Fisher Scientific, Florence, KY), 1% antibiotic/antimycotic solution and 1% L-glutamine. Plates were kept in a cell culture incubator under standard conditions (37°C, 5% CO_2, 100% humidity, dark) for 28 days. Every 3–4 days, all media was removed and replaced. Bright field light microscope photographs of the wires in media were taken at 28 days using a Zeiss Stemi 2000-C dissecting scope with a Zeiss Axiocam Mr C camera (Zeiss).

***In vitro* release of Mg: Analysis with Xylidyl Blue assay.** The free Mg ion concentration in media extracts from the *in vitro* degradation experiment was measured with a Xylidyl Blue assay (based on a commercial kit from Stanbio, Boeme, TX).[16] Media and reference samples (concentration curve of $MgCl_2$ solutions) were diluted (1/20 in water) and pipetted into wells containing reagent (100 μL of sample added to 1 mL of Xylidyl Blue reagent). The dye reagent solution contained Xylidyl Blue (0.1 m*M*), Tris buffer (200 m*M* pH = 11), ethelene glycol-bis(B-Aminoethyl ether)-N,N,N′,N′-tetraacetic acid (EGTA) (0.1 m*M*), and distilled water. A spectrophotometric plate reader (Spectramax) and its software (SoftMax Pro Data) (both from Molecular Devices, LLC, Sunnyvale, CA) were used to detect the absorbance at 520 nm, which increased with increasing Mg^{++} content. Readings were taken within 30 min of combining reagents. Three segments of each wire were used and four media samples were tested per wire, per day of analysis. The data sets were exported and processed in Microsoft Excel and SigmaPlot (Systat Software, Inc.). Data are expressed as the concentration of free Mg^{++} above that of the control medium (0.8 m*M* in the complete medium). If not specified, all other materials were from Thermo Fisher Scientific.

Scanning electron microscopy and energy dispersive X-ray analysis of Mg wires after *in vitro* degradation. After 28 days of immersion in culture medium, wires were embedded in silicone, cut in cross section and sputter coated with a thin (<50 nm) layer of Au/Pd alloy to prevent charging. Wires were placed in the scanning electron microscopy (SEM; XL-30 ESEM, FEI/Phillips, the Netherlands) chamber and examined using SEM and energy dispersive X-ray (EDX; at 30 kV) modes.

Subcutaneous implantation in adult mice

A total of 14 mice (female C57/Bl6, 6 weeks, Jackson Labs, Bar Harbor, ME) were used for subcutaneous placement of wires. All animal treatment protocols were approved by the University of Cincinnati Institutional Animal Care and Use Committee (IACUC) and were in accordance with the Animal Welfare Act and the NIH Guide for the Care and Use of Laboratory Animals. Wire sections (0.5 cm long) of both Mg and SS were prepared and sterilized as above. Mice were anesthetized using isofluorane gas, given analgesics and monitored during and after surgery. Two wires per mouse were inserted into small pockets created under the skin on the back of the mouse, one on either side of the backbone (three mice per condition, except for 375°C, where two mice were implanted). Wounds were covered with Tegaderm© (3M Company, St. Paul, MN, for up to 14 days). No signs of discomfort, infection or skin reaction were observed. At 28 days after implantation, animals were euthanized and the skin covering the lower half of the back (approx. 1.5 in. × 1 in.) was removed and fixed (4% paraformaldehyde in phosphate buffered saline [PBS]). Not all wires were found at sacrifice, perhaps due to either corrosion or loss through the skin (although no signs of skin penetration were detected). Within 2–4 h of sacrifice, skin samples were placed into a PBS filled holder and imaged via micro-computed tomography (micro-CT).

Micro-CT imaging after subcutaneous implantation. Dissected skin samples with wires were imaged via micro-CT imaging using an Inveon Multimodality System (Siemens, Knoxville, TN) in the University of Cincinnati Vontz Imaging Core Lab. The samples (several per scan) were kept moist in PBS (~1 h scan), as shown previously for another preparation.[6] Scanning of samples was done as previously described.[6] Briefly, scanning used half-degree increments with 384 steps (step and shoot) for 192°, and the effective voxel size was 17.27 μm. The Inveon Research Workplace was used for 2D and 3D analysis, for creation of 3D volume rendered images, to crop the images of each skin sample into separate files and to export as DICOM files (Digital Imaging and Communications in Medicine, the universal digital format agreed upon for use by all human medical imaging manufacturers). Images were created using Inveon, NIH ImageJ and Photoshop software.

Histology. Immediately after micro-CT imaging, the skin samples were returned to fixative for 1 day, rinsed (PBS) and stored in 70% EtOH until embedded in paraffin, cut into 8 μm sections and mounted on slides. Slides were stained with hematoxylin and eosin (H&E) or Masson's Trichrome stain (Trichrome, Newcomer Supply, Middleton, WI). Adjacent slides were immunostained for nerves (rabbit anti-protein S100, stains Schwann cells, 1:500, Dako, Carpenterio, CA), axons (rabbit anti-200MW neurofilament protein (NF200), 1:500 dilution, Sigma-Aldrich) and, following

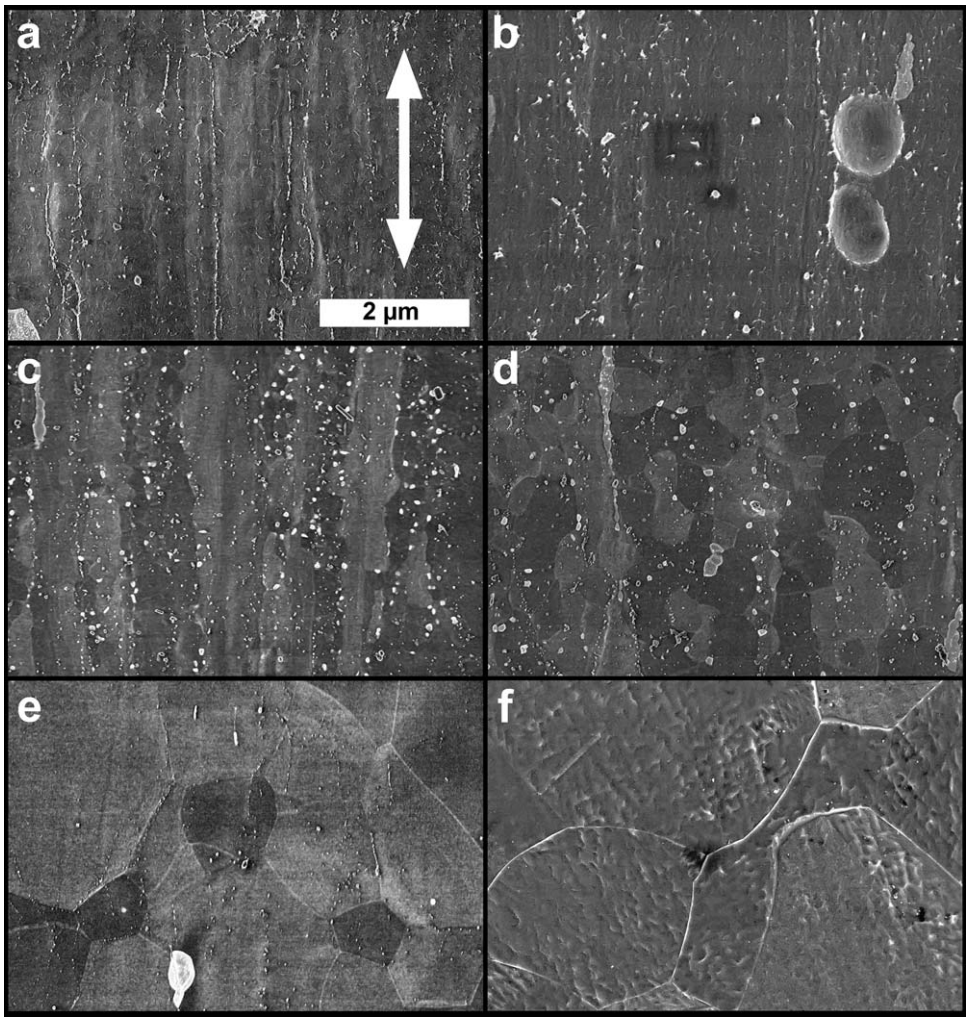

FIGURE 1. Microstructural assessment. Combined secondary and backscattering electron micrographs of the wires at different treatment conditions, (a) CW, (b) 250°C, (c) 375°C, (d) 400°C, (e) 450°C, and (f) SS. The top-bottom directions of all the graphs are aligned with the drawing direction. Bar = 2 μm, applies to all.

proteinase K (Sigma-Aldrich) antigen retrieval, macrophages (the F4/80 (mouse monoclonal) pan-macrophage antibody, 1:500, Abcam, Cambridge, MA), as per standard methods.[6] Secondary antibodies were goat anti-mouse Alexa 488 and goat anti-rabbit Alexa 594 (1:1000, Life Technologies, Carlsbad, CA, 2 h). Cell nuclei were labeled with 4′,6-diamidino-2-phenylindole (DAPI, diluted 1:1000 in secondary antibody, Sigma Aldrich). Tissues were coverslipped with Fluoromount.

Photography of sections and image analysis. Photomicrographs were taken on an upright Zeiss Axioplan Imaging 2e fluorescence microscope. Color bright field images were taken with a Zeiss Axiocam digital camera. Fluorescence images were taken in black and white, in three channels, with a QICam cooled CCS camera (Q Imaging, Canada) and combined into composites and pseudo colored using Photoshop (Adobe Systems Inc.). Cavity areas (left by Mg wire) were measured using NIH ImageJ in sections stained with either H&E or Masson's Trichrome. Calculated diameters were compared across Mg wire conditions (from all except the 375°C condition, where only one wire was retrieved) ($n = 14$ wires total, 3–4 wires per condition, 3–20 images averaged per wire, $n = 110$ images).

Statistics

Statistical analyses were done using SigmaPlot v13, with a significance level of $p < 0.05$ and blinded conditions. Error bars show standard deviations. For analyses of variances (ANOVAs), if data were significant and distributed normally, the Holm–Sidak method was used for pairwise multiple comparisons. Repeated measures one- or two-way ANOVAs were used where appropriate.

RESULTS

Microstructural assessment

In the CW condition, most grains were highly elongated from the drawing process, and around 0.2 μm in the transverse dimension (Figure 1a). Some fine secondary-phase precipitates were observed, often in the form of long

TABLE I. Tensile Properties of Five WE43B Wire TMP Conditions

TMP Condition	Yield Strength (MPa)	Ultimate Tensile Strength (MPa)	Elongation (%)	Elastic Modulus (GPa)
CW	492 ± 2	521.6 ± 0.4	2.4 ± 0.2	34.3 ± 0.2
250°C	579 ± 4	608.3 ± 0.5	2.8 ± 0.2	35.4 ± 0.3
375°C	479.1 ± 0.6	495.1 ± 0.6	5.9 ± 0.7	35.2 ± 0.2
400°C	397.3 ± 0.6	411.7 ± 0.3	10.9 ± 0.2	35.1 ± 0.2
450°C	298 ± 3	325 ± 2	11 ± 2	32.4 ± 0.3

"stringers." Annealing at 250°C led to larger and more pronounced secondary phases (Figure 1b). There was very limited grain growth, and the elongated fiber structures were less apparent. Annealing at temperatures between 375 and 450°C (Figure 1c–e) resulted in a noticeable growth in the transverse grain dimension (from approximately 1 μm at 375°C to 3 μm at 450°C) and increasing elimination of fiber structures as the annealing temperature went higher, with grains being completely equiaxial at 450°C (Figure 1e). In comparison, SS wire exhibited equiaxial grain structure with grain size ranging from 1 to 5 μm (Figure 1f).

Tensile testing

Tensile testing of the five TMP conditions of WE43B wire revealed a wide range of mechanical behavior (Table I and Figure 2). The CW condition exhibited very high strength at 522 MPa, but a low elongation in tension at 2.4%. Aging the material at 250°C increased the strength beyond 600 MPa, but again had a low elongation of only 2.8%. Increasing heat treatment temperature from 375 to 400 and 450°C resulted in decreases in strength with increases in tensile elongation.

Surgical handling assessment

To test the potential for surgical use, wires were tied into knots and ranked using simple metrics (Table II), that included number of knots withstood before wire fracture (related to flexural toughness) and ease of forming knots (related to elasticity). These metrics informed the general usability for simple surgical procedures such as suturing. Three of the five TMP conditions (CW, 400 and 450°C) were found to be usable for suturing, while the other two (375 and 250°C) were considered unusable.

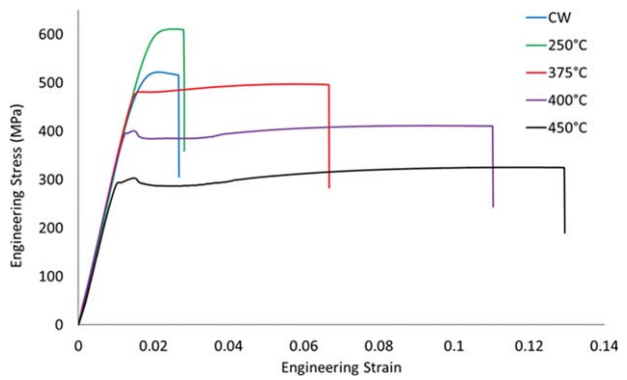

FIGURE 2. Tensile data. The 127 μm WE43B wires exhibited a wide range of tensile properties depending on TMP condition.

Wire corrosion *in vitro*

To examine Mg corrosion *in vitro*, under conditions as close as possible to physiological conditions, Mg wire samples were immersed for 28 days in a standard culture medium (with serum), under cell culture conditions, for 28 days. Media samples were tested for free Mg^{++} content (Mg release) per media change and cumulative Mg release (Figure 3). All conditions showed the greatest release of Mg at 4 days *in vitro* (4 DIV). There were no significant differences between conditions at 4 DIV (Figure 3a, one-way ANOVA, $p = 0.729$) or at any subsequent day (Figure 3b, repeated measures two-way ANOVA (RMA), $p = 0.87$ for condition and $p = 0.947$ for interactions between condition and day). Cumulative release was calculated and graphed (Figure 3c), and total release after 28 DIV showed no significant differences between conditions (Figure 3d, ANOVA, $p = 0.649$). There was a trend toward lower release for the CW condition at 4 DIV and in total cumulative release.

Scanning electron microscopy and energy dispersive X-ray analysis of Mg wire corrosion *in vitro*. After 28 days, samples of each wire were embedded in silicone, cut and visualized via SEM. The wires were fragile and friable, as demonstrated by extensive cracking and breakage of the surfaces (Figure 4, column 1).

Selected areas on each wire (red rectangles) were analyzed for elemental composition by EDX spectroscopy. Data from two areas, one representing the outer edge and one the central area, are given in Figure 4, columns 2 and 3 (Supporting Information gives the data for all areas). The areas might contain corrosion precipitates of Mg, which would include oxides, phosphates, and carbonates because of reaction with the medium components. Major differences between the TMP conditions occurred in the relative weight percentages (wt %) of Mg in the central core versus edge of wires, as illustrated by the bar graphs (Figure 4, column 2) and numerical data (Figure 4, column 3). The two annealed (400 and 450°C) and the 375°C wires had virtually no Mg in their cores, with slightly more on the edges, suggesting a hollow shell configuration. The major component in the cores for these samples was silicone, suggesting that the embedding material had filled up the core. In contrast, the CW and 250°C samples contained distinctly higher percentages of Mg in the core than in the edge. Based on the relative wt %, the CW and 250°C wires retained the most Mg in their core areas, while the wt % of Mg for all other areas, both core and edge, for all wires, was very low (<10%).

TABLE II. Handling Characteristics of Five WE43B Wire TMP Conditions, Based on Usability for a Basic Suturing Procedure

TMP Condition	# Knots	Handling Characteristics	Usability
CW	1–2	Elastic, high yield strength leads to stiff feel	Usable
250°C	0	Highly elastic and brittle	Unusable
375°C	0	Elastic and relatively brittle, though improved over 250°C	Unusable
400°C	3–4	Some elasticity but less than CW	Usable
450°C	3–4	Very similar to 400°C	Usable

Light microscopic analysis of wire corrosion *in vitro.* After 28 DIV and prior to embedding in silicone, pieces of the Mg wires were photographed using bright field light microscopy, and these views showed very different patterns of corrosion between conditions (Figure 5). The light microscopic images were consistent throughout the wires for the 250, 400, and 450°C conditions and the relative densities are consistent with the EDX analyses. The 400 and 450°C conditions resulted in hollow shells, consistent with the EDX result showing primarily silicone in the center, while the 250°C wire appeared to have the greatest extent of dark material in the center. For the two conditions showing variable densities along their lengths (CW and 375°C), the EDX analyses presumably reflected sections taken through the areas indicated by arrows in Figure 5.

Subcutaneous implantation in adult mice

Micro-CT imaging after subcutaneous implantation. To analyze *in vivo* corrosion, sections of Mg and control SS wire were implanted under the skin of mice for 28 days, then the skin containing wires was imaged via micro-CT. Figure 6a–c shows representative longitudinal micro-CT views that are reconstructions of sequential axial views. The views showed that at least one of each treatment was broken (four or six wires per treatment). Significant bending of wires was only seen for the 450°C treatment (in two of five wires recovered) and for SS wires. Only one wire out of four implanted was recovered in the 375°C condition and it had the highest fragmentation. All wires appeared solid, in contrast to the wires maintained *in vitro*. Areas of presumably localized pitting were observed, as indicated by corrosion products appearing as protuberances on the wire

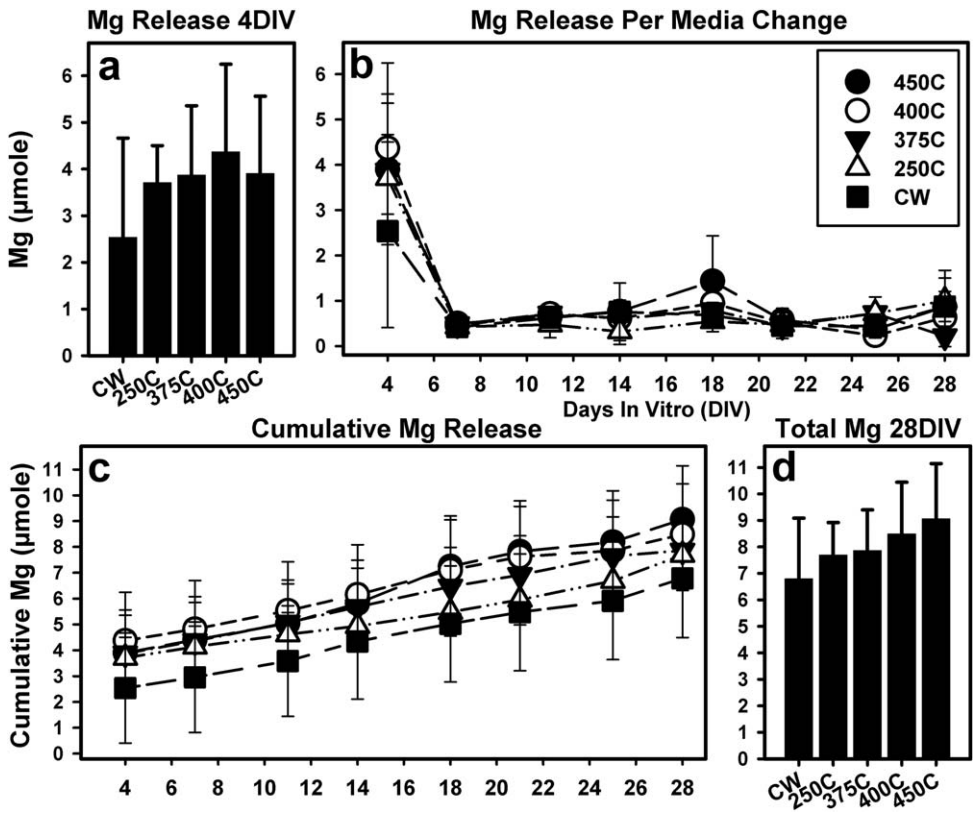

FIGURE 3. Release of Mg^{++} by WE43B wires into culture medium over 28 days *in vitro*, under cell culture conditions. (a) Release at the first media change, at 4 DIV, was not different between wire conditions. (b) Mg release was also not different between conditions at subsequent days. (c) Cumulative Mg release (µmoles per wire, 1 mL of medium). (d) No significant differences were seen for total Mg release after 28 days.

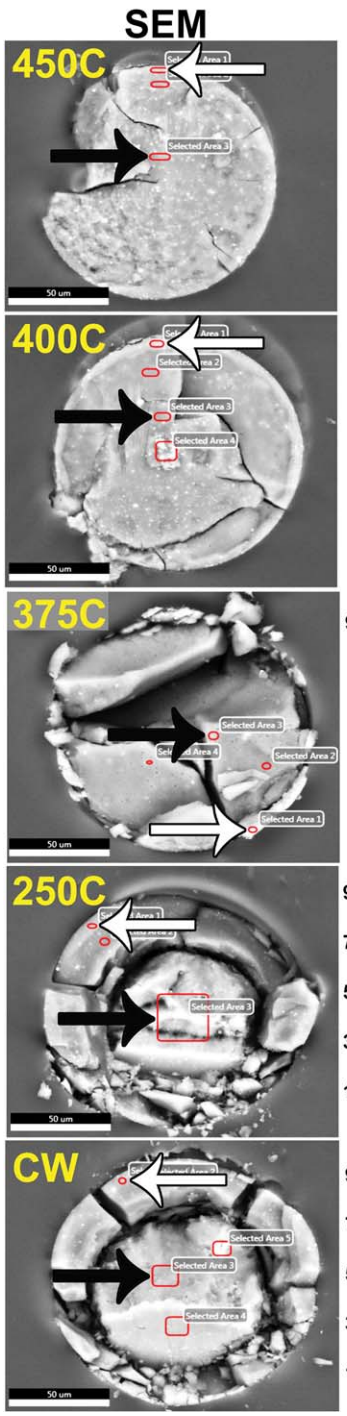

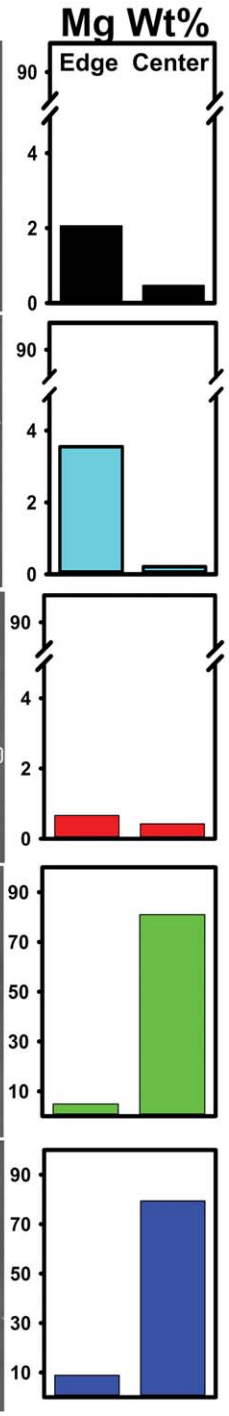

Element	Edge	Center
C	25.95	9.9
Ca	8.98	27.88
Mg	2.06	0.47
Nd	1.2	5.91
O	36.47	23.63
P	9.41	14.09
Si	14.64	18.13

C	11.13	17.54
Ca	15.02	9.91
Mg	3.55	0.21
O	43.52	33.06
P	11.07	7.6
Si	8.17	21.62
Y	4.11	6.58

C	26.55	19.51
Ca	6.02	6.85
Mg	0.66	0.42
Nd	1.02	2.76
O	39.41	34.21
P	7.8	10.38
Si	17.53	24.46

C	10.96	5.17
Ca	13.52	0
Mg	4.86	80.99
O	46.86	1.77
P	10.55	0.44
Si	8.44	2.1
Y	3.5	6.83

C	7.6	6.76
Ca	10.27	0
Mg	8.84	79.4
O	47.83	3.52
P	11.33	0.52
Si	5.91	2.25
Y	6.61	3.24

FIGURE 4. SEM and EDX analysis of Mg wires after *in vitro* corrosion in culture medium for 28 days. (Column 1) SEM images. The areas in the red rectangles on each SEM were analyzed by EDX. The arrows on the images in column A indicate the two areas per wire that are described in columns 2 and 3. Black arrows indicate spots analyzed for central portions of each wire, while white arrows indicate the spots analyzed on the edge areas. (Column 2) The EDX results for the two areas per wire are shown in the graphs that compare the weight percentage of Mg (wt %) in one edge versus one central spot area, per wire. (Column 3) The tables give the wt % of the most abundant elements in each edge and center area, for each condition.

(Figure 6, arrowheads). In general, it appeared the wires experienced localized fracture but not substantial bulk corrosion.

Histological assessment. After micro-CT imaging, skin samples were embedded in paraffin and stained with H&E (Figure 7a), Masson's Trichrome stain (Figure 7b) or immunostained (Figure 7c,d) for macrophages (green) and nerves (labeling for Schwann cells, red). Cavities appeared where the Mg wire had been washed out or dissolved during processing (asterisks in Figure 7), sometimes leaving what appeared to be degradation products (Figure 7a). Cavity

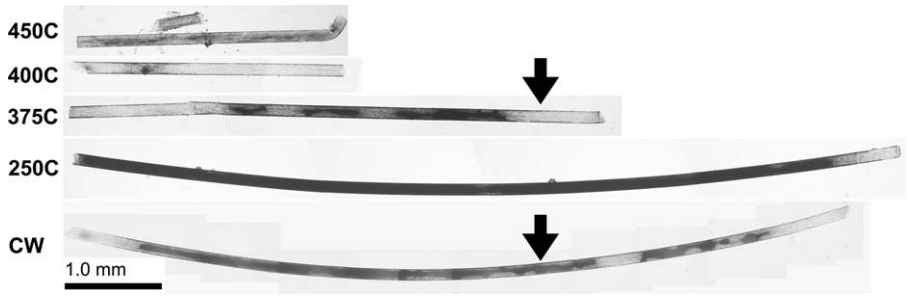

FIGURE 5. Light micrographs of Mg wires after *in vitro* corrosion in culture medium for 28 days. Arrows for CW and 375°C conditions indicate regions that appear to be similar to the areas analyzed by SEM/EDX and shown in Figure 4.

areas were measured and the diameters did not vary across four conditions (CW, 250, 400, and 450°C, ANOVA, $p = 0.614$). The average diameter ($n = 14$ wires) was 127.58 ± 7.65 μm, which is indistinguishable from the original diameter of 127 μm. The maximum and minimum diameters were only 33 and 27% of the average (169 and 93 μm, respectively, $n = 110$ images). Dewaxed sections examined by SEM and EDX showed no evidence of Mg in tissues surrounding the wires (Supporting Information). These data corroborate the micro-CT data and show that the wires were not corroding as rapidly *in vivo* as they had *in vitro*.

The tissue reaction to the wires was formation of a capsule around the wire that consisted of layers of tightly packed cells adjacent to the Mg, followed, outside that, by concentric layers of fibroblasts and collagen (blue in Trichrome stain) that then blended into adjacent connective tissue. The collagen density was variable between and along wires, but never reached the density seen in the dermis. Cells in the tightly packed layer appeared to be primarily macrophages, but not all were F4/80 positive (green cells in Figure 7c,d), which is expected as expression is dependent on macrophage type and maturation status.[17] Foreign body giant cells were rare (not shown). The lymphocytic infiltration in the capsule layers was similar to that in adjacent connective tissue, without dense accumulations. Blood vessels were abundant within and adjacent to the capsule. Measurements of the area of tightly packed cells adjacent to the cavity showed no major differences between conditions (ANOVA, $p = 0.098$, for the four conditions (as above), $n = 3$–4 wires per condition, averages of 2–6 images per wire). The average wall thickness was 24.6 ± 5.3 μm (average over 40 images) and maximum and minimum values were 36.3 and 16.1 μm. Overall, all evidence suggested a uniform and mild foreign body reaction to all wire conditions.

Large nerve bundles were present in the connective tissue adjacent to the Mg wires (arrowheads, Figure 7c,d), but no specific association with the wires was observed. However, smaller nerve fibers were unusually abundant in the dense capsular material (arrow in Figure 7d) (also seen after staining for a neurofilament protein, not shown).

DISCUSSION

This study is the first to investigate the influence of TMP conditions on corrosion and handling in fine Mg alloy wire. Mg

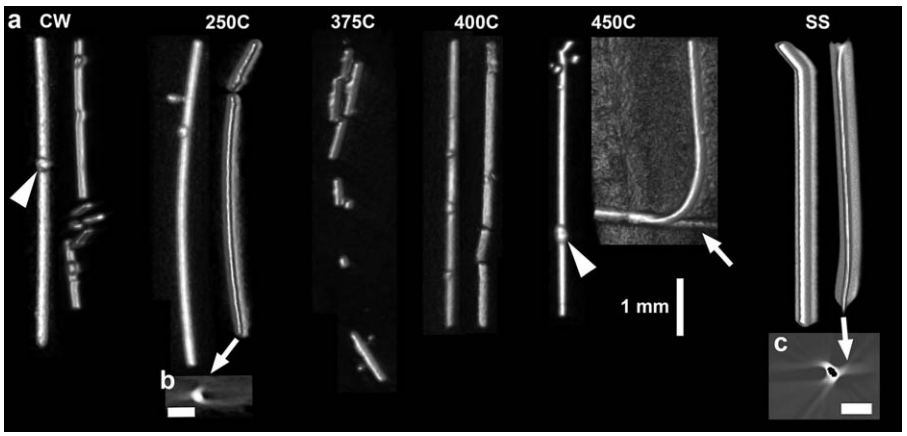

FIGURE 6. Micro-CT of Mg wires after *in vivo* implantation for 28 days. All wires (imaged while embedded in skin) appeared solid and relatively uniform in diameter. (a) Longitudinal micro-CT reconstructions (two per condition, except 375°C). Arrowheads point to bulges. Bar = 1 mm, applies to all. Inserts (b) and (c): ridges on some longitudinal views appeared to be imaging artifacts, probably due to reflections, based on both axial views (arrows point from longitudinal views to inserts showing representative axial views) and because ridges were not seen in subsequent histological views. Bars = 500 μm in axial views. Other imaging artifacts included anomalous densities (arrow points to a bar in one 450°C image). Shadows indicating skin surrounding wires were detectable at certain contrast levels (450°C, bent wire).

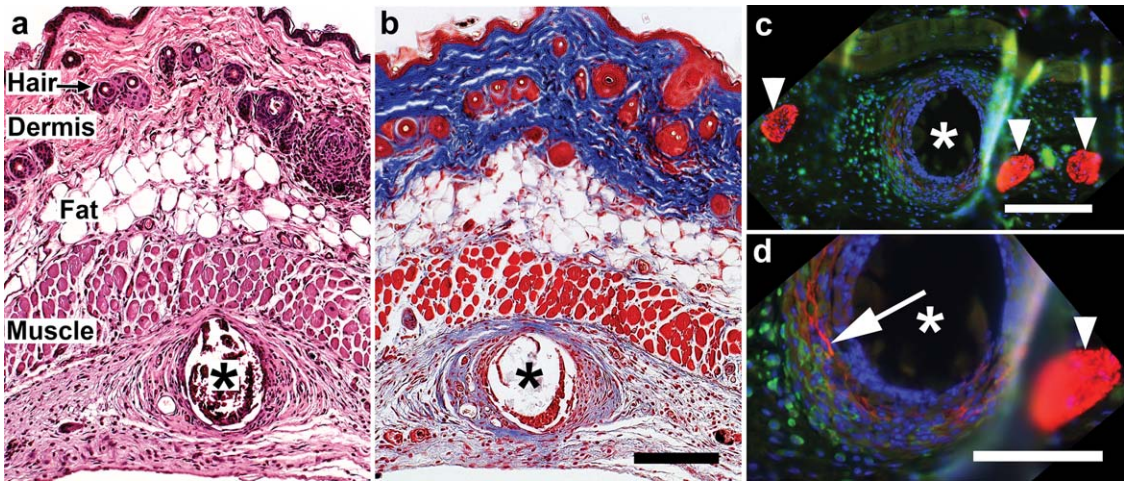

FIGURE 7. Histology of Mg wires in mouse skin after *in vivo* implantation for 28 days. Asterisks indicate the cavity left by the Mg wire. (a) H&E staining (450°C wire). Layers (top to bottom) are epidermis (dense line at top), dermis containing hair follicles (arrow), a layer of fat, the panniculus muscle layer (muscle) and then connective tissue, where the Mg wires had been placed. (b) Adjacent section stained with Masson's Trichrome. Collagen stains blue, muscle, and cellular cytoplasm are red and nuclei are dark blue. Bar = 150 μm (applies to (a, b)). (c) Sections (250°C wire) were stained for macrophages (F4/80 antibody, in green), Schwann cells surrounding nerve axons (anti-S100 protein, red) and nuclei (DAPI, blue). Arrowheads (c, d) point to large nerve fascicles, typical in this layer. Bar = 150 μm. (d) Higher magnification of the section shown in (c). Bar = 100 μm. Thinner nerve bundles (arrow) were detected in the denser connective tissue surrounding the Mg cavity.

may be ideally suited for immediate, temporary support for soft tissue repair as the wealth of evidence in the literature points to safe absorption without significant inflammatory reaction, provided excessive corrosion and hydrogen generation are avoided.[18] Various medical devices may require tailored degradation profiles to match the needs of the local tissues.

The wide range of mechanical properties obtained in the WE43B wires with different TMP conditions highlights the ability to tune mechanical properties to specific applications, as has been reported previously.[8,19] As shown in the surgical handling test, only the CW, 400°C, and 450°C TMP conditions were deemed suitable for the suture knotting application, while the 250 and 375°C conditions were unsuitable. In knotting, bending ductility and toughness are required to prevent fracture. With the high tensile elongation of the annealed conditions, it is not surprising they performed well in the knotting test. The relatively low yield strength also leads to improved shape-retention of the knot. It is counter-intuitive that the cold-worked wire also performed well in knotting, given that the elongation in tension was the lowest of all five TMP conditions. However, this is consistent with other highly cold-worked wire materials used in accepted medical applications, such as pacing leads.[20] The gradient stress field generated by bending may allow for greater deformation than the uniform stress seen in a tensile test.

With traditional, nonabsorbing wires, it is generally sufficient to ensure appropriate mechanical performance and the effects of corrosion can be neglected. With absorbable materials, however, the corrosion behavior must be considered as well. *In vitro* test methods are useful in screening candidate alloys and processes, and to identify mechanistic behaviors, but *in vivo* tests are always necessary for absorbable device development due to the myriad parameters that can affect absorption.[3,14] In-service environmental conditions, such as local blood perfusion (which determines metal access to physiological salt solutions) and mechanical loading (which may lead to stress-corrosion cracking) must be understood. Further, scholarly reporting of both *in vitro* and *in vivo* test data with identical materials is a critical activity if the field is to one day approach an *in vitro–in vivo* correlation.

The Xylidyl Blue assay confirmed the release of Mg ions but was unable to distinguish between TMP conditions. It is likely that the relatively small volume of wire led to low Mg ion concentrations which were at the lower limit of the assay's detection abilities.

The visual and EDX examination of corrosion after *in vitro* immersion tests proved more useful in differentiating TMP conditions in *in vitro* corrosion. Light microscopy indicated the 400 and 450°C conditions corroded more rapidly than the others, and this was confirmed by EDX, showing very low percentages of remnant Mg. The CW and 250°C conditions showed dense core material remaining by light microscopy, and the highest percentages of Mg by EDX. Light microscopy also indicated the 375°C condition had undergone non-uniform corrosion, with an inconsistent profile along the length. The EDX data in this condition was collected from a region having had relatively high corrosion. While the EDX data are not quantitatively precise, they are qualitatively accurate and provide useful information on the local material state.

The relatively low corrosion rate of the materials with highly elongated grains (CW, 250°C, and 375°C) is an interesting finding. While understanding the mechanism behind this is beyond the scope of this study, the authors speculate it could be related to the ultrafine transverse diameters and the resulting fiber structure. Further testing with the

material under stress is warranted to inform the risk for stress-corrosion cracking in these high-stored-energy conditions.

After subcutaneous implantation, bulk corrosion rates were slower than in cell media. The lack of diameter reduction (as measured by both micro-CT and histology) suggests that significant corrosion had not occurred. This discrepancy between *in vitro* and *in vivo* corrosion is consistent with earlier findings, likely owing in part to the rapid attachment of fibroblasts and macrophages to the metal surface and subsequent reduction of exposure to physiological salt solutions.[3,14] Notably, the overall degradation rate of the 127 μm WE43B wires examined in this work appears to be advantageously slower than that of the 250 μm commercially pure Mg wires studied previously.[6] In that study, the pure Mg wires were largely dissolved after 6 weeks in a regenerating nerve environment.

While limited bulk corrosion occurred in the WE43B wires after 4 weeks of subcutaneous implantation, differences between TMP conditions were observed in terms of wire fragmentation. The 375°C condition showed the greatest fragmentation in the one sample that was located. The other three may have entirely corroded, migrated away from the wound region, or protruded through the skin. The bending observed in some 450°C condition is reflective of its low yield strength and high ductility.

No significant negative tissue reaction was observed in any TMP condition. This is unsurprising, as all wires had the same chemical makeup and no major differences in bulk corrosion rates and associated ion release were found. Interestingly, multiple small nerve fibers within the capsular material adjacent to wire implants were observed. Previous literature has suggested nerve fiber interactions with implants, but efforts to quantify such interactions have been relatively limited and inconsistently applied.[21] Examination of nerve fibers around Mg wire implants may be more reliable than with nonabsorbable metal implants, as Mg wires are soft enough to section using conventional histological means. This is a worthy avenue of future research, as recent reports showed that Mg implants in bone stimulate neurotransmitter release from adjacent peripheral nerve fibers.[22]

In view of the numerous assessments in the study, the 450°C may be most suitable for surgical knotting procedures. Although the strength was lowest of the five TMP conditions, and the *in vitro* corrosion was among the most rapid, the highly favorably surgical handling response and reduced fragmentation risk *in vivo* make it the most promising for this procedure, with the 400°C condition close behind. The CW condition had suitable knottability, good strength, and a low *in vitro* corrosion rate, but was more prone to fragmentation than the 450°C condition *in vivo*. The 250 and 375°C treatments would not be suggested for medical applications like knotting which require plastic deformation during surgery but could find use in applications requiring high elasticity, such as self-expanding braided stents.

CONCLUSION

This work shows that fine WE43B wires can be tuned by processing to exhibit a wide range of mechanical properties with varying corrosion behavior. This work also contributes to the large body of evidence documenting the difficulty in achieving *in vitro–in vivo* correlation, with reduced wire corrosion rates observed *in vivo*. The data presented herein serve as a foundation for further development of devices tailored to specific applications.

ACKNOWLEDGMENTS

The authors thank the UC SEM facility and Dr. Melodie Fickenscher for help with SEM and EDX and the UC Vontz Core Imaging Laboratory and Kathlyn LaSance for help with micro-CT imaging and interpretation and Catherine Beaucage and Xiaoxian An for technical assistance.

REFERENCES

1. Luthringer BJC, Willumeit-Römer R. Effects of magnesium degradation products on mesenchymal stem cell fate and osteoblastogenesis. Gene 2016;575:9–20.
2. Waizy H, Seitz J, Reifenrath J, Weizbauer A, Bach F, Meyer-Lindenberg A, Denkena B, Henning W. Biodegradable magnesium implants for orthopedic applications. J Mater Sci 2013;48:39–50.
3. Zheng YF, Gu XN, Witte F. Biodegradable metals. Mater Sci Eng R Rep 2014;77:1–34.
4. Windhagen H, Radtke K, Weizbauer A, Diekmann J, Noll Y, Kreimeyer U, Schavan R, Stukenborg-Colsman C, Waizy H. Biodegradable magnesium-based screw clinically equivalent to titanium screw in hallux valgus surgery: Short term results of the first prospective, randomized, controlled clinical pilot study. Biomed Eng Online 2013;12:1–10.
5. Di Mario C, Griffiths H, Goktekin O, Peeters N, Verbist J, Bosiers M, Deloose K, Heublein B, Rohde R, Kasese V, Ilsley C, Erbel R. Drug-eluting bioabsorbable magnesium stent. J Intervent Cardiol 2004;17:391–395.
6. Vennemeyer JJ, Hopkins T, Hershcovitch M, Little KD, Hagen MC, Minteer D, Hom DB, Marra K, Pixley SK. Initial observations on using magnesium metal in peripheral nerve repair. J Biomater Appl 2015;29:1145–1154.
7. Griebel AJ, Schaffer JE. Development of high-strength bioabsorbable mg alloys suitable for conventional cold-working processes. Eur Cell Mater 2013;26(Suppl 5):2.
8. Griebel AJ, Schaffer JE. Cold-drawn ZM21 and WE43 wires exhibit exceptional strength and ductility. Eur Cell Mater 2014;28:2.
9. Griebel AJ, Schaffer JE. Fatigue performance of Resoloy® magnesium alloy wire. Presented at 8th Symposium on Biodegradable Metals, May 14–17, 2016, L'Estérel resort, Laurentide, Montréal, Canada.
10. Song G. Control of biodegradation of biocompatible magnesium alloys. Corros Sci 2007;49:1696–1701.
11. Gu XN, Zhou WR, Zheng YF, Cheng Y, Wei SC, Zhong SP, Xi TF, Chen LJ. Corrosion fatigue behaviors of two biomedical mg alloys—AZ91D and WE43—In simulated body fluid. Acta Biomater 2010;6:4605–4613.
12. Liu D, Ding Y, Guo T, Qin X, Guo C, Yu S, Lin S. Influence of fine-grain and solid-solution strengthening on mechanical properties and in vitro degradation of WE43 alloy. Biomed Mater 2014;9:1–9.
13. Witte F, Kaese V, Haferkamp H, Switzer E, Meyer-Lindenberg A, Wirth CJ, Windhagen H. In vivo corrosion of four magnesium alloys and the associated bone response. Biomaterials 2005;26: 3557–3563.
14. Durisin M. Bioabsorbable behaviour of magnesium alloys—An in vivo approach. In: Surface Modification of Magnesium and Its Alloys for Biomedical Applications, Vol 1. Elsevier Ltd, New York, NY; 2015. pp 123–178.
15. Semiatin SK. Recovery, recrystallization, and grain-growth structures. In: Semiatin SK, editor. ASM Handbook Materials Park, OH

14A: Metalworking: Bulk Forming. ASM International; 2005. pp 552–562.
16. Chromý V, Svoboda V, Štepánová I. Spectrophotometric determination of magnesium in biological fluids with Xylidyl Blue II. Biochem Med 1973;7:208–217.
17. Austyn JM, Gordon S. F4/80, a monoclonal antibody directed specifically against the mouse macrophage. Eur J Immunol 1981;11: 805–815.
18. Zhao D, Witte F, Lu F, Wang J, Li J, Qin L. Current status on clinical applications of magnesium-based orthopaedic implants: A review from clinical translational perspective. Biomaterials 2017; 112:287–302.
19. Griebel AJ, Schaffer JE. Fatigue and corrosion fatigue of cold drawn WE43 wires. Magnes Technol 2015:303–307.
20. Schaffer JE. An examination of fatigue initiation mechanisms in thin 35Co-35Ni-20Cr-10Mo medical grade wires. J ASTM Int 2008; 7:1–10.
21. Huang Y, Jacobs R, Van Dessel J, Bornstein MM, Lambrichts I, Politis C. A systematic review on the innervation of peri-implant tissues with special emphasis on the influence of implant placement and loading protocols. Clin Oral Implants Res 2015;26:737–746.
22. Zhang Y, Xu J, Ruan YC, Yu MK, O'Laughlin M, Wise H, Chen D, Tian L, Shi D, Wang J, Chen S, Feng JQ, Chow DHK, Xie X, Zheng L, Huang L, Huang S, Leung K, Lu N, Zhao L, Li H, Zhao D, Guo X, Chan K, Witte F, Chan HC, Zheng Y, Qin L. Implant-derived magnesium induces local neuronal production of CGRP to improve bone-fracture healing in rats. Nat Med. 2016;22:1160–1169.